Pure appl. geophys. 165 (2009) 2019–2044
0033–4553/08/112019–26
DOI 10.1007/s00024-008-0414-9

Pure and Applied Geophysics

Numerical Modeling and Observations of Tsunami Waves in Alberni Inlet and Barkley Sound, British Columbia

Isaac V. Fine,[1] Josef Y. Cherniawsky,[1] Alexander B. Rabinovich,[1,2]
Fred Stephenson[1]

Abstract—Alberni Inlet is a long and narrow fjord adjacent to Barkley Sound on the Pacific Coast of Vancouver Island, Canada. Port Alberni, at the head of the inlet, was affected in 1964 by the largest Pacific tsunami waves in Canadian history. We use observations and results from two numerical models to investigate the resonant characteristics of the region and amplification of tsunami waves in Barkley Sound and Alberni Inlet. The first model (A) was forced at its open boundary with a stationary autoregressive signal, similar to the observed background noise. The second model (B) used an initial sea-level deformation from a potential earthquake off California in the southern segment of the Cascadia Subduction Zone, producing transient tsunami waves. Spectral, cross-spectral and frequency-time (*f-t*) analyses of the observations were used to examine the resonant properties and topographic response of the local area. The respective results show large admittance functions over a wide 0.5–0.9 cph frequency band, implying a low *Q* factor but high amplification of arriving waves. This unusual behavior is a result of two effects: A quarter-wave resonance of the system for its fundamental Helmholtz mode and amplification due to the narrowing of the channel cross section from Barkley Sound to Alberni Inlet. The model A numerical results agree favorably with the observations, indicating an energetic resonant mode at frequency of $\sim$0.53 cph (112 min), with its nodal line located near the entrance to Barkley Sound and amplification factor value close to 12. The results from the tsunami propagation model (B) yield spectral characteristics similar to those from the model A and from the observations. The maximum tsunami current speed for this scenario is 2.4 ms^{-1} in Sproat Narrows, which divides Alberni Inlet into two parts, while the largest computed wave height is 1.6 m in the northern Alberni Inlet, in the area of Port Alberni.

Key words: Port Alberni, 1964 Alaska tsunami, tsunami modeling, tide gauge records, resonant oscillations, seiches, cross-spectral analysis.

1. Introduction

Alberni Inlet is a long ($\sim$40 km) and narrow (1–2 km) fjord located on the west coast of Vancouver Island on the Pacific Coast of Canada (Fig. 1). This fjord is the longest on the island and is characterized by a deep (>250 m) southern part of the channel but

[1] Institute of Ocean Sciences, Fisheries and Oceans Canada, 9860 West Saanich Rd., Sidney, BC V8L 4B2, Canada. E-mail: Josef.Cherniawsky@dfo-mpo.gc.ca

[2] Russian Academy of Sciences, P.P. Shirshov Institute of Oceanology, 36 Nakhimovsky Prosp., Moscow 117997, Russia.

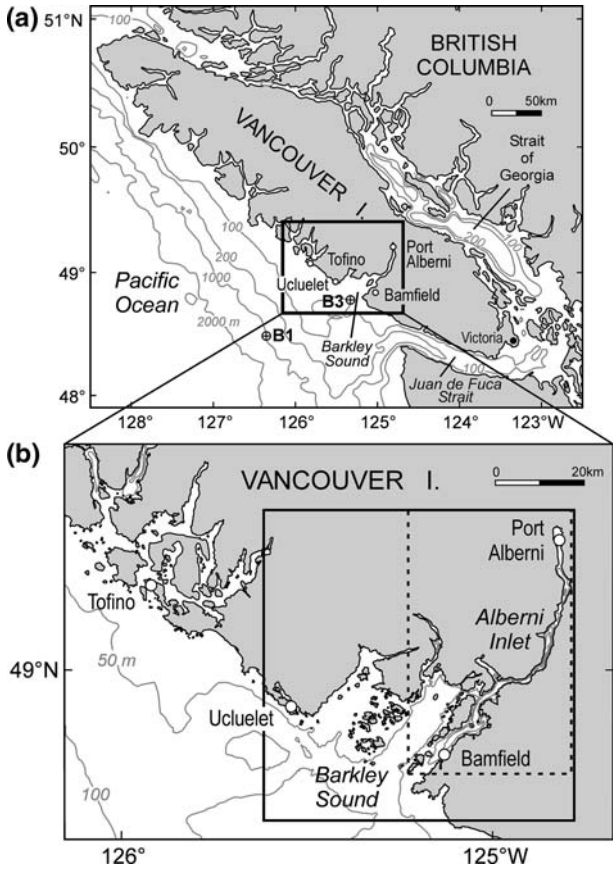

Figure 1
(a) Map of the area of Vancouver Island (British Columbia) shown with depth contours and locations of tide gauges in Tofino, Bamfield, Port Alberni and Victoria. The symbols ⊕ mark locations of sea-level timeseries at B1 (1000 m depth) and B3 (85 m). (b) Map of Barkley Sound and Alberni Inlet showing domains of the two numerical models: Model A (solid frame), which was used to examine characteristic wave properties of the Barkley Sound–Alberni Inlet system, and the innermost grid of model B (dashed frame), used for modeling tsunami waves.

relatively shallow ($\sim$100 m) approaches in the relatively wide Barkley Sound located between the inlet and the continental shelf. On March 28, 1964, the town of Port Alberni, at the head of the inlet and about 65 km from the open Pacific Ocean, experienced the largest tsunami waves on the coast of Vancouver Island, generated by the 1964 ("Good Friday") Alaska Earthquake (M_w = 9.2). These waves caused wide-spread flooding and property damage estimated to be about 10 million (1964) dollars (WHITE, 1966; CLAGUE, 2001; CLAGUE *et al.*, 2003; ANDERSON and GOW, 2004). However, alarms were sounded, people were rescued from flooded homes and there was no loss of life in Port Alberni. Notably, this Pacific-wide tsunami was responsible for close to 130 deaths and about 125

million dollars in damage in Alaska, Washington, California and Hawaii (SPAETH and BERKMAN, 1967; LANDER, 1996; STEPHENSON *et al*., 2007). This tsunami was recorded by twelve tide gauges on the Pacific Coast of Canada (cf. WIGEN and WHITE, 1964; WIGEN, 1983; STEPHENSON *et al*., 2007), including the tide gauges at Tofino, located northwest of Barkley Sound, at Port Alberni in Alberni Inlet, and at Victoria, inside Juan de Fuca Strait (Fig.1).

The 1964 tsunami was destructive at several locations on the coast of Vancouver Island (CLAGUE *et al.,* 2003; ANDERSON and GOW, 2004; STEPHENSON *et al.,* 2007), with the highest wave in Canada occurring at Shields Bay, on the west coast of Graham Island (Queen Charlotte Islands), where a wave crest was reported to be 5.2 m above spring high water, or 9.8 m above tidal datum (SPAETH and BERKMAN, 1967; STEPHENSON *et al.,* 2007). However, most of the damage occurred in Port Alberni, where wave heights exceeded 8 m. The Port Alberni tide gauge was disabled temporarily and stopped working several times before the wave height maxima were reached (Fig. 2a), but according to witness reports, the second wave was the highest in the series, reaching 6.4 m above tidal datum, as was determined from water marks on buildings and harbor structures. This can be compared to a maximum wave height of 2.4 m in Tofino (STEPHENSON *et al.,* 2007). The resulting flooding and property damage in Port Alberni

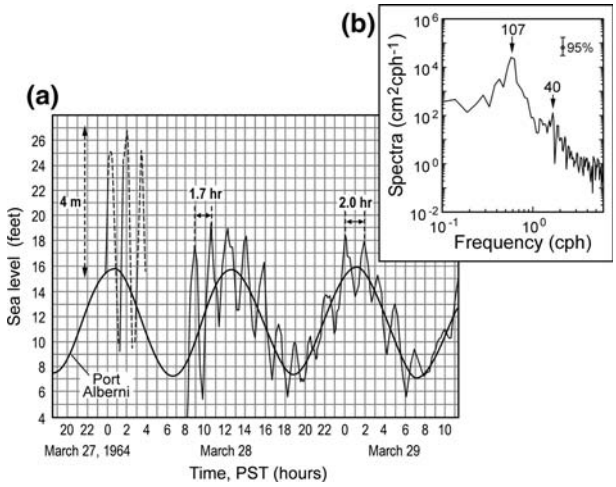

Figure 2

(a) A restored copy of Port Alberni tide gauge record of the Alaska tsunami of March 28, 1964 (from WIGEN and WHITE, 1964). Predicted tide is shown by a thick line. The tide gauge stopped working on March 28 after 04:00 PST, and resumed operation four hours later. The highest recorded sea level, about 4 m above high tide at 02:00 PST, was due to a second incoming tsunami wave, while the corresponding maximum (peak-to-through) wave height at Port Alberni was about 6 m, or larger, and occurred during the third, or a later wave. The exact count and the maximum wave height of the largest tsunami wave are uncertain because of the 4-hour data gap. Oscillations in Alberni Inlet persisted for at least 48 hours, with wave periods from 1.7 to 2 hours. (b) Computed spectrum of the tsunami record at Port Alberni shown in (a) for the time period between 08:00 28 March and 10:00 29 March. Periods (in min) of two main spectral peaks are indicated.

were made worse by the fact that the first two waves arrived around the time of high water tide (Fig. 2a).

A number of questions arose from this catastrophic event. What is the physical mechanism responsible for the destructive tsunami oscillations observed in Port Alberni? Why did such strong oscillations occur specifically in this inlet? Which tsunami waves (local or distant) are likely to cause significant future damage in this area?

Significant tsunami oscillations in Port Alberni (as well as at other B.C. stations) continued for several days, being highly regular and almost monochromatic, with wave periods between 1.7 and 2 hours (Fig. 2a). It was therefore naturally assumed that the 1964 event in Alberni Inlet had a resonant character (cf. Murty and Boilard, 1970; Murty, 1992; Henry and Murty, 1995). The averaged wave spectrum at Port Alberni (Fig. 2b) shows a dominant peak with a period of approximately 1.8 hours ($\sim$107 min). Such a strong response was likely due to the fact that this spectral peak is near the fundamental period of the inlet.

Several numerical models were constructed to simulate tsunami wave propagation in the northeastern Pacific Ocean and wave transformation on the continental shelf, including the shelf of Vancouver Island (cf. Hebenstreit and Murty, 1989; Dunbar *et al.,* 1991; Whitmore, 1993; Myers and Baptista, 2001; Cherniawsky et al., 2007). A number of studies (Murty and Boilard, 1970; Henry and Murty, 1972; 1995; Kowalik and Murty, 1993) were focused specifically on explaining the observed 1964 tsunami oscillations in the Alberni Inlet. However, the spatial resolution of these models and the accuracy of the bathymetry were insufficient for the region with such complicated topography. These models also did not allow to resolve the detailed frequency spectrum and relative amplification of the long-wave oscillations in the inlet. Finally, the lack of high-quality digital records of tsunamis and background oscillations was a key factor limiting the ability to estimate the frequency characteristics of the wave field in the region and to verify the numerical tsunami models in this area.

The destructive tsunamis of the 1990s in the Pacific Ocean initiated a major upgrade of the existing Tsunami Warning system and of the Permanent Water Level Network (PWLN) on the coast of British Columbia. New digital instruments were introduced to continuously measure sea-level variations with 1-min sampling. During the period 1999–2007, long time series of such high quality sea-level data were collected at a number of stations, including Tofino and Bamfield, and several weak tsunamis were recorded by these instruments (Rabinovich and Stephenson, 2004; Stephenson *et al*., 2007; Stephenson and Rabinovich, 2008). At the outset of 2006, a digital tide gauge was installed at Port Alberni, replacing an older analogue tide gauge used at this site during 1961–1997. This new and precise instrument provided us with reliable two-year long time series of the background oscillations at the head of Alberni Inlet, and measured a weak tsunami from the Kuril Islands earthquake (M_w = 8.3) of 15 November, 2006 (Stephenson *et al*., 2007). In addition, we re-examined historical analogue recordings of tide gauges on the BC coast and identified four tsunamis during 1994–1996 that were observed at several sites, including Port Alberni (Stephenson and Rabinovich, 2008).

These new tsunami and sea-level background data are used here to estimate the spectral properties of oscillations in the inlet and to verify the numerical model results.

We used two numerical models to investigate the resonant characteristics of the Barkley Sound and Alberni Inlet system and to examine transformation and amplification of tsunami waves arriving from the open ocean. The first model (A) was forced at its open boundary with a stationary autoregressive (AR) signal, similar to the observed background wave noise. This was an updated and improved version of the model that was used to investigate the resonant oscillations in the bays and inlets of the Kuril and Balearic Islands (DJUMAGALIEV *et al*., 1994; RABINOVICH *et al*., 1999). The second model (B) used an initial sea-level deformation from a potential earthquake off California, in the southern segment of the Cascadia Subduction Zone, to produce transient tsunami waves arriving at the shelf of Vancouver Island and then propagating inside Barkley Sound and Alberni Inlet. A similar model was used successfully to estimate sea-level variations and associated currents in bays and harbors of the southern and southwestern coast of Vancouver Island (CHERNIAWSKY *et al*., 2007). Results from these models are compared with actual observational data.

2. *Observations of Tsunamis*

The 1964 Alaska tsunami was the strongest tsunami ever recorded in Port Alberni and on the Pacific Coast of Canada. However, there were also records of other tsunamis in Alberni Inlet; although all of them were relatively small (other major Pacific Ocean tsunami events, such as Aleutian 1946, Kamchatka 1952 and Chile 1960, were not recorded due to the absence of a tide gauge in Port Alberni). The most complete information on tsunamis at Port Alberni, as well as at other locations on the BC coast, can be found in the catalogue by STEPHENSON *et al.* (2007).

Four tsunamis were identified in the analogue records of the BC tide gauges for the period of 1994–1996 (STEPHENSON *et al*., 2007; STEPHENSON and RABINOVICH, 2008), with the corresponding earthquakes listed in Table 1.

All four tsunamis were recorded at Port Alberni, as well as at several other BC stations, including Tofino and Bamfield (see Figs. 30–33 in STEPHENSON *et al.*, 2007).

Table 1

Earthquakes in the Pacific Ocean (1994–1996) which generated tsunamis recorded on the BC coast

Date	Region	M_w
04 October 1994	Kuril Islands, Russia	8.3
30 July 1995	Northern Chile	8.0
03 December 1995	Kuril Islands, Russia	7.9
17 February 1996	Irian Jaya Region, Indonesia	8.2

Tide gauge records at these three sites for the Kuril Islands 1994 and 1995 events are shown in Figure 3. Tsunami waves are evident in Figure 3 and the arrival times of these waves are relatively clear. Other important features of these observations are:

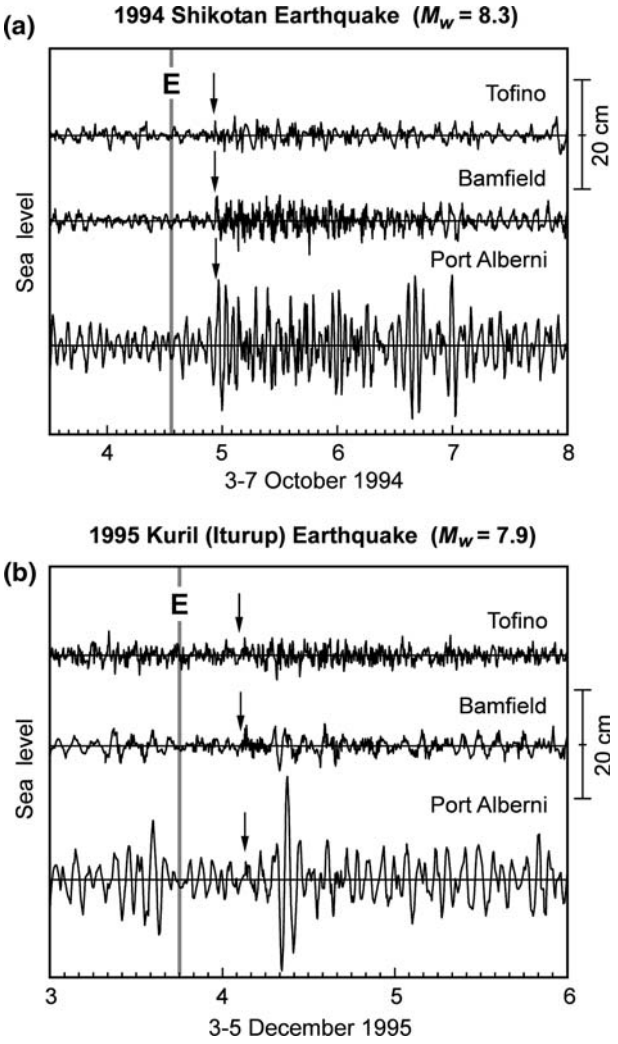

Figure 3

Tsunami records from three tide gauges (Tofino, Bamfield and Port Alberni) located on the west coast of Vancouver Island for two trans-Pacific tsunamis: (a) From a 1994 Shikotan earthquake ($M_w = 8.3$) and (b) from the 1995 Kuril (Iturup) earthquake ($M_w = 7.9$). "E" denotes the time of the main earthquake shocks, while arrows depict the tsunami arrival time.

(a) Tsunami ringing is relatively long, longer than 2–3 days, and their energy decay is slow.
(b) The maximum wave heights at Port Alberni are 3–4 times larger than at Tofino or Bamfield and are more often in a third (e.g., in 1964), or a later wave.
(c) The dominant oscillations at Port Alberni are more regular and have lower frequencies than at the other stations.

It is likely that these features and the differences between various sites are determined by local topographic effects.

To examine transient behavior at frequencies of the observed tsunami waves, we used the multiple-filter technique (EMERY and THOMSON, 2001). This method is similar to wavelet analysis and was developed to study nonstationary signals whose time series exhibit temporal changes in amplitude and/or phase. It uses narrow-band filters and a Gaussian window which isolates a specific center frequency $\omega_n = 2\pi f_n$. Demodulation of a sea-level time series $\zeta(\omega_n; t)$ yields a matrix of amplitudes and phases of wave signals, with columns representing the time and rows the frequency (the so-called *f-t* diagrams). This method is used effectively to examine tsunami records and to analyze tsunami wave energy $E(f, t)$ as a function of frequency and time (cf. RABINOVICH *et al.*, 2006).

Figure 4 presents *f-t* diagrams for the 1994 Shikotan and the 1995 Kuril Islands (Iturup) tsunami records at Bamfield and Port Alberni. Most of the energy in these plots is at low frequencies (periods of 60–180 min). The arrival of tsunami waves from the 1994 earthquake is clearly seen as an increase in the energy level at all frequencies at Bamfield and for periods exceeding about 20 min at Port Alberni. For this event, there were no pronounced oscillations prior to the tsunami arrival. Specifically, the incoming tsunami wave energy induced significant seiche oscillations observed at these two sites.

In contrast, the 1995 Kuril (Iturup) tsunami wave was weaker (Fig. 3b) and its arrival was masked by existing background ocean wave noise, as noticeable background oscillations were observed before the tsunami arrival. Tsunami waves introduce additional energy and are further amplified at discrete frequencies that correspond to the natural oscillations, or standing wave modes of an inlet or a harbor. Such resonant modes are usually numbered in the order of frequency, starting from the gravest ($n = 0$) fundamental mode. In particular, an increase in the energy at tsunami arrival time is apparent in Figure 4 for a period of $\sim$110 min. Except for this minor difference, the *f-t* diagrams for these two events are very similar.

The diagrams in Figure 4 demonstrate that the tsunami wave energy is concentrated mostly in the same frequency bands as the energy for the background long-wave oscillations. This feature of tsunami waves plays a key role in the coastal water response to the arriving tsunami waves (cf. MILLER, 1972). Specifically, there is resonant generation and amplification of local seiches when the periods of the incoming waves match the characteristic (natural) periods of the site. Conversely, a non-resonant response is observed when there is a pronounced mismatch in these periods. Three distinct

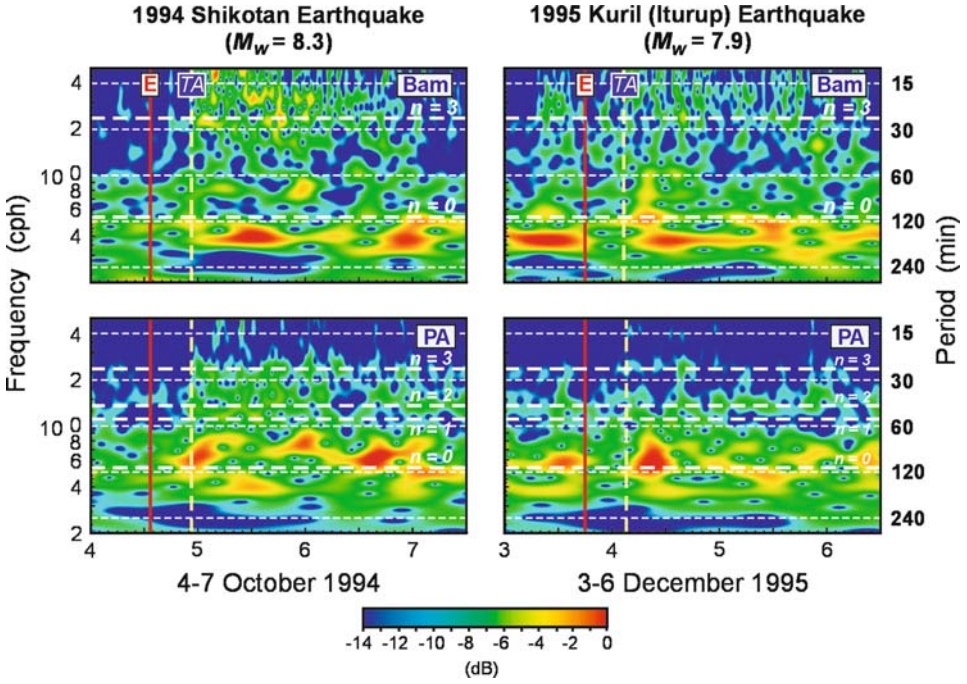

Figure 4
Frequency-time plots (*f-t* diagrams) for the 1994 Shikotan and the 1995 Kuril (Iturup) tsunamis from tide gauge records at Bamfield (Bam) and Port Alberni (PA). The vertical red line labelled "E" denotes the time of the main earthquake shock, while the dashed vertical yellow line labelled "*TA*" marks the estimated tsunami arrival time. Thick dashed horizontal lines mark the frequencies and periods of characteristic modes; two (n = 0, 3) modes were marked for Bamfield and four (n = 0, 1, 2, 3) for Port Alberni (these modes were computed by the model A, as is explained below).

frequency bands, with peak periods of approximately 110, 43 and 23 min, are evident in the *f-t* diagrams for Port Alberni (Fig. 4). As shown in the next two sections, these bands are related to the characteristic modes of the Alberni Inlet – Barkley Sound system. Two of the frequency bands, with periods of 110 min and 23 min, are also apparent in the *f-t* diagram for Bamfield. These plots reveal an obvious tsunami wave-train (packet) structure; the duration of each wave train is 12 to 18 hours.

3. *Observations of Background Noise*

To determine the spectral properties of longwave oscillations in the Barkley Sound – Alberni Inlet system and to compare these properties at various sites, we analyzed 2-month-long records of background oscillations (with 1-min sampling) at Port Alberni, Bamfield and Tofino. The spectral procedure used is similar to that described in EMERY and THOMSON (2003). To improve our spectral estimates, we used a Kaiser-Bessel spectral

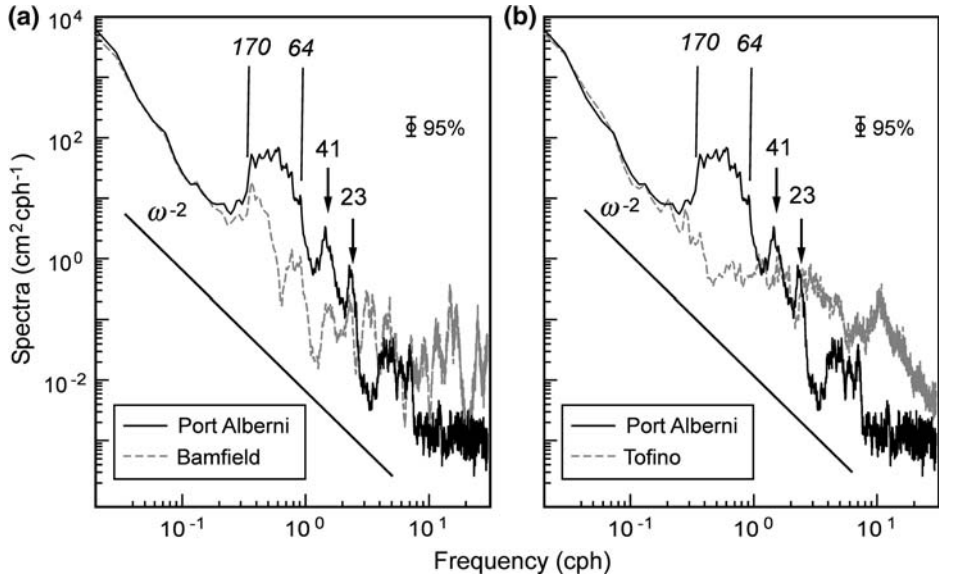

Figure 5
Comparison between the spectra of background sea-level oscillations: (a) at Bamfield and Port Alberni, (b) at Tofino and Port Alberni. Periods (in min) of the main peaks are indicated.

window, with half-window overlaps, prior to applying the Fourier transform. The width of the window was chosen to be 4096 min (~68.3 h), yielding about 80 degrees of freedom per spectral estimate. The results are shown in Figure 5. For comparison, we present in Figure 5a the spectrum for Port Alberni together with that for Bamfield, while in Figure 5b we show the spectra for Port Alberni and for Tofino.

The general forms of the background spectra for Port Alberni, Bamfield and Tofino are similar and for wave periods longer than 3 hours, the three spectra are almost identical. These spectra are "red," as their spectral energy decreases with increasing frequency, with their slope proportional to ω^{-2}, which is typical for long-wave sea-level spectra in the open ocean (cf. KULIKOV *et al.*, 1983; FILLOUX *et al.*, 1991; RABINOVICH, 1997). The long ocean waves are transformed as they propagate from the open ocean onto the shelf and along the shore. Their spectra become more energetic and "jagged" with decreasing depth and when approaching the coast (cf. Fig. 1 in RABINOVICH, 1997).

The spectrum of background atmosphere-induced waves near the coast can be described as (RABINOVICH, 1997):

$$S_b(\omega) = S_0(\omega)\, Q_b(\omega)\; P_b(\omega), \tag{1}$$

Where Q_b is the admittance function for a shelf (which can also include a bay, or a gulf, similar to Barkley Sound), P_b is the inlet/harbor admittance function and S_0 is the open ocean background spectrum. The remarkable feature of $S_0(\omega)$ is that it is usually smooth

and monotonic and has no distinct spectral peaks. Thus, individual peaks and troughs in the observed spectra $S_b(\omega)$ are related to topographic features.

While tsunami waves have larger amplitudes than the background waves, their transformation on the shelf and in bays and harbors is mostly linear, except in very shallow bays and during on-shore run-up (e.g., Titov and Synolakis, 1993; Satake, 1995). Thus, admittance functions and other spectral characteristics of the tsunami waves can be studied by comparison with the spectra of background noise.

The spectral characteristics of Alberni Inlet are of primary interest for the present study. In general, the background spectrum at Port Alberni (Fig. 5) looks similar to the spectrum of the 1964 tsunami wave at this site (Fig. 2b). However, the background spectrum has considerably better resolution ($\sim$0.015 cph) and thus contains far more detail.

The most interesting and important feature of this spectrum is the wide spectral rise in the frequency range of 0.35–0.94 cph (periods of 64–170 min). It is worth emphasizing that the high resolution of this spectrum ensures that this rise is the physical property of the system and not related to insufficient spectral resolution. The corresponding rise is mostly absent in the spectra for Tofino and Bamfield. It is therefore likely that this rise is mainly due to the influence of Alberni Inlet. At the same time, this spectral feature is significantly different from typical spectra of long-wave oscillations in long and narrow inlets, or in bays and harbors with narrow entrance, which normally have a strong and narrow spectral peak associated with the fundamental Helmholtz mode of the basin, as was observed, for example, in Malokuriskaya Bay, Kuril Islands (Djumagaliev *et al.*, 1994; Rabinovich, 2008), or in Citadella Inlet, Balearic Islands (Rabinovich *et al.*, 1999; Rabinovich, 2008; Vilibić *et al.*, 2008).

The strong broadening of the spectral peak at Port Alberni may be partly due to the influence of Barkley Sound (Fig. 1). This is supported by a particular feature of the spectrum at Bamfield (located near the entrance to Barkley Sound), which has a peak with a period near 170 min, matching the frequency of spectral energy increase at Port Alberni (Fig. 5a). In contrast, the spectrum at Tofino (located to the north of Barkley Sound) has no such peak (Fig. 5b).

Other noteworthy features of the Port Alberni spectrum (Fig. 5) are the peaks at 1.45 cph (41.5 min) and 2.61 cph (23 min). The Bamfield spectrum peaks (Fig. 5a) are similar to those at Port Alberni, although with less energy. The similarity of the background spectra at Port Alberni and Bamfield indicates that these two sites are part of a common system, influenced by similar basin modes. In contrast, the Tofino spectrum (Fig. 5b) is very different from those at Bamfield and Port Alberni. Therefore, sea-level oscillations at Tofino are essentially independent from those in Barkley Sound and in Alberni Inlet.

At higher frequencies (periods less than 23 min), the Port Alberni spectrum decreases more rapidly than the Bamfield and Tofino spectra. Oscillations at Bamfield and Tofino at these frequencies appear to be related to local seiches. Several high-frequency peaks (with periods of 2.4, 3.5, 5 and 18 min at Bamfield and 5.6 and 12 min at Tofino) are observed in these spectra (Fig. 5). Similar peaks were also observed at these sites during

the 2001 Peru, 2001 Queen Charlotte and 2004 Sumatra tsunami events (RABINOVICH and STEPHENSON, 2004; RABINOVICH *et al.*, 2006).

4. Numerical Model A: Background Waves in Barkley Sound and Alberni Inlet

To examine long-wave background oscillations in the Barkley Sound–Alberni Inlet system, we used a linear shallow-water equations numerical model (so-called "model A"). Its finite-difference formulation is similar to that in the TUNAMI N2 model (IMAMURA, 1996).

The model was forced by prescribed incident waves at its open boundaries, which have "red noise" spectra, similar to the observed background noise. A stationary autoregressive (AR) model of the first order was used for this purpose:

$$\zeta_0^j = a\zeta_0^{j-1} + \varepsilon, \tag{2}$$

where $\zeta_0^1, \zeta_0^2, \ldots, \zeta_0^{j-1}$ are the input wave elevations, a is the regression coefficient ($0 < a < 1$), and ε is a random process of the "white noise" type. The normalized spectrum of (2) has the form

$$S_\zeta(\omega) = [1 - 2a\cos(\omega\Delta t) + a^2]^{-1}, \tag{3}$$

where Δt is the sampling interval of the input time series. The spectrum (3) is a monotonic function of ω, which for $\omega\Delta t \ll 1$, decreases according to a ω^{-2} power law, similar to the observed background spectra in the open ocean (KULIKOV *et al.*, 1983; FILLOUX *et al.*, 1991; RABINOVICH, 1997). The original version of this model was used to examine the resonant oscillations in the bays and inlets of Shikotan Island (Kuril Islands) (DJUMAGALIEV *et al.*, 1994) and Menorca Island (Balearic Islands) (RABINOVICH *et al.*, 1999).

There are two main advantages in applying such a model. First, and in contrast to a common method based on numerical simulation of monochromatic waves with select frequencies (cf. HENRY and MURTY, 1995), the present model is forced at its open boundary using waves with a continuous spectrum. This allows us to calculate the system response over a complete frequency range. Second, this model time series of simulated sea levels can be examined using the same spectral and cross-spectral analyses as for the observed time series. The simulated and observed time series and their spectra can then be compared in great detail and also used for the verification of the model.

The computational domain for this model is shown in Figure 1b. Its grid dimensions are 1213 × 1223 and (x, y) grid size is 50 m. The time step used was 0.53 s.

Model sea-level time series were computed and stored for Port Alberni and Bamfield. These time series were used in cross-spectral analysis, for estimation of coherence, phase differences and admittance functions between the two sites. Similar analyses were also performed on the two-month long time series of observed sea levels at these two locations.

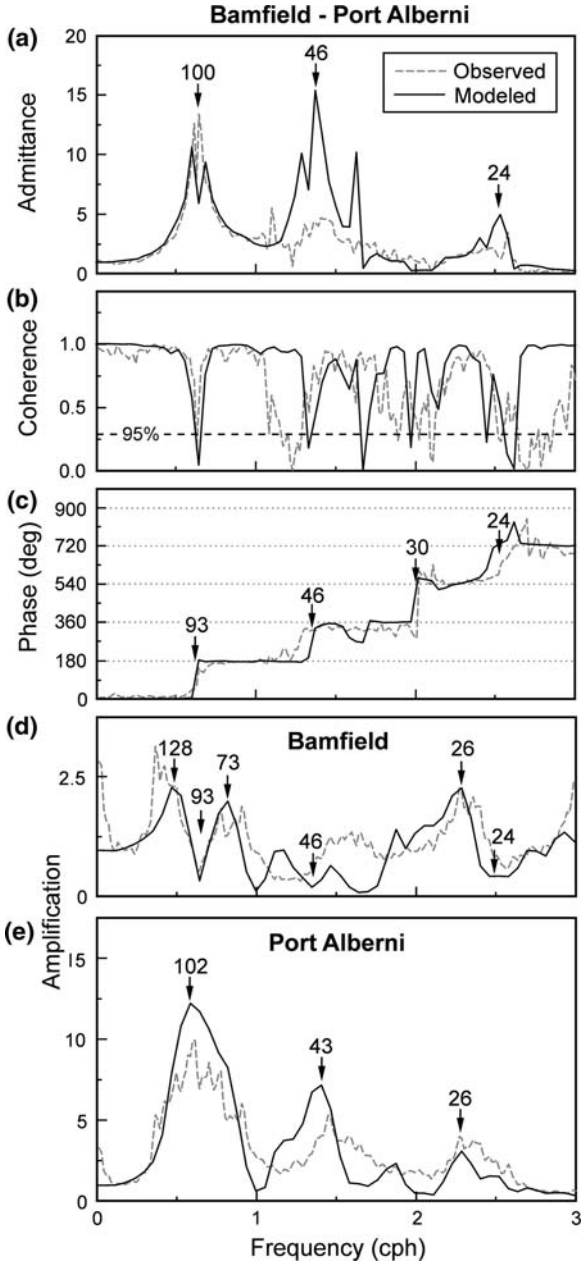

Figure 6

Characteristics of the cross-spectra between Bamfield and Port Alberni for the observed and the model A simulated sea-level oscillations: (a) admittance, (b) coherence and (c) phase difference. Periods (in min) of the main peaks are indicated. Observed and the model A simulated amplification factors: (d) at Bamfield, (e) at Port Alberni. Periods (in min) of the main peaks and troughs are indicated.

The model was integrated for 10 days using above random forcing at its open boundary, providing sufficiently long quasi-stationary time series for standard spectral analyses. To verify the model performance, we compared between the observed and the modeled Bamfield – Port Alberni cross spectra (Fig. 6).

In general, admittance, coherence and phase spectra show a very good agreement with the observations in the frequency range of up to 2.5 cph. This is especially true for the model phase spectrum, which is nearly identical to the observed (Fig. 6c). The modeled admittance is close to the observed up to 1 cph. However, the level of the modeled peak at 46 min (1.3 cph) is much higher than observed (Fig. 6a), which is likely due to a standing wave node being located near Bamfield at this frequency in the model. This peak is not as prominent in the observations at Bamfield, as it is masked by additional non-coherent noise.

The remarkable agreement in Figure 6 between the simulated and the observed spectra for Bamfield and Port Alberni suggest that this model is sufficiently reliable and can provide realistic results not just for these two stations but for the entire area.

Cross-spectral analysis of the observed sea-level variations at Port Alberni and Bamfield (Fig. 6) provides additional insight, beyond the features shown by the autospectra in Figure 5a. The admittance function in Figure 6a has prominent peaks at approximately the same frequencies as in the Port Alberni spectrum (Fig. 5a), however the admittance peaks are sharper and more pronounced than the spectral peaks. The coherence is high over the entire frequency range of 0.0–3.0 cph (i.e., at periods longer than 20 min), except for some narrow and abrupt troughs (Fig. 6b).

Phase differences between the two sites are step-like, with phase shifts near 0° or 180° (Fig. 6c). These shifts correspond exactly to the frequencies of the coherence minima. The cross-spectral coherence and phase plots indicate that oscillations in Alberni Inlet and in the adjacent Barkley Sound are due to standing waves in the system. Therefore, phase shifts and coherence minima are related to the nodes moving past Bamfield and into the inlet with increasing frequency. Indeed, the Bamfield spectrum (Fig. 5a) shows minima at these transition frequencies.

The cross-spectral characteristics between Bamfield and Port Alberni sea-level records (Fig. 6) confirm the general features of the Port Alberni spectrum (Fig. 5), with additional peaks corresponding to the minima observed at the Bamfield spectrum. The first node is near Bamfield at 0.63 cph (95 min), inside the 0.5–1 cph frequency band of the broad Port Alberni spectral peak. This means that a maximum amplitude response in Alberni Inlet (near 0.6 cph) corresponds to the first ($n = 0$) fundamental mode, with node location further offshore from Bamfield, probably close to the mouth of Barkley Sound.

From (1), we calculate the observed wave amplification $A(\omega)$ at Port Alberni and Bamfield:

$$A(\omega) = \sqrt{Q_b(\omega)\, P_b(\omega)} = \sqrt{S_b(\omega)/S_0(\omega)}, \tag{4}$$

where $S_0(\omega) = (\omega_0^2/\omega^2)\, S(\omega_0) = C/\omega^2$. ω_0 is a reference frequency (chosen here ω_0 = 0.25 cph) and C is a constant related to the open ocean spectra, computed from Figure 5 as $C = 0.125$ cm^2 h^{-1} = 3.5×10^{-9} m^2 s^{-1}.

For the model simulated records, we calculate the amplification function as:

$$A_M(\omega) = 0.5\sqrt{S_M(\omega)/S_{0M}(\omega)}, \tag{5}$$

where $S_M(\omega)$ is sea-level spectrum at a particular location and $S_{0M}(\omega)$ is the spectrum of the prescribed incident (forcing) waves. The coefficient 0.5 in equation (5) ensures that the modeled amplification factor is equal to unity at low frequencies, as is the case for the observed waves.

The modeled amplification functions show a good agreement with the observations both for Bamfield and for Port Alberni (Figs. 6d, e). The main features of these functions are similar for both locations, as was also indicated by the high coherence between Bamfield and Port Alberni (Fig. 6b). Amplification at Port Alberni (Fig. 6e) is relatively high for periods from 70 to 120 min. Another maximum in amplification, though smaller in value, is near the 43-min period.

Amplification at Bamfield (Fig. 6d) shows similar, though much smaller peaks. The main peak at 0.5–1 cph is split into two peaks due to a spectral minimum near 0.6 cph (see Fig. 5a). As was explained above, this minimum corresponds to the position near Bamfield of the first node at this frequency (Figs. 6a-c). Amplification at Bamfield also shows additional (in comparison to Port Alberni) minima at wave frequencies higher than 1 cph, when the nodes of these waves are located near Bamfield.

The first minimum (at 93 min) in Figure 6d is the same for both the observed and the modeled spectra. However, the minimum at a 46-min period appears only in the modeled function, with the observed function showing a broad minimum from about 55 to 45 min. These differences in amplification are consistent with the differences between the modeled and the observed admittance functions (Fig. 6a).

Spatial distribution of the response is shown in Figure 7 for six selected frequencies. At 0.4 cph, the Barkley Sound–Alberni Inlet system shows relatively weak amplification, with no nodes (lines of zero amplitude) present in Figure 7a. As the frequency increases, amplification sharply increases inside Alberni Inlet and Barkley Sound, reaching a maximum at 0.53 cph (113 min). This maximum in amplification corresponds to a nodal line near the entrance to Barkley Sound (Fig. 7b). With further frequency increase, this first node moves into the inlet and amplification in Alberni Inlet remains high up to 0.73 cph (Figs. 7c to 7e). As this node moves past Bamfield and inside Alberni Inlet, the oscillations in Alberni Inlet and in Barkley Sound have an opposite phase. When frequency reaches 0.93 cph, the amplitudes decrease sharply and the oscillations are weak everywhere (Fig. 7f).

Figure 8 provides yet another description of the model frequency response, showing the spatial structure of the three main modes (Fig. 8a) and relative sea levels (amplification) for frequencies up to 2 cph (Fig. 8b) along a transect from Barkley

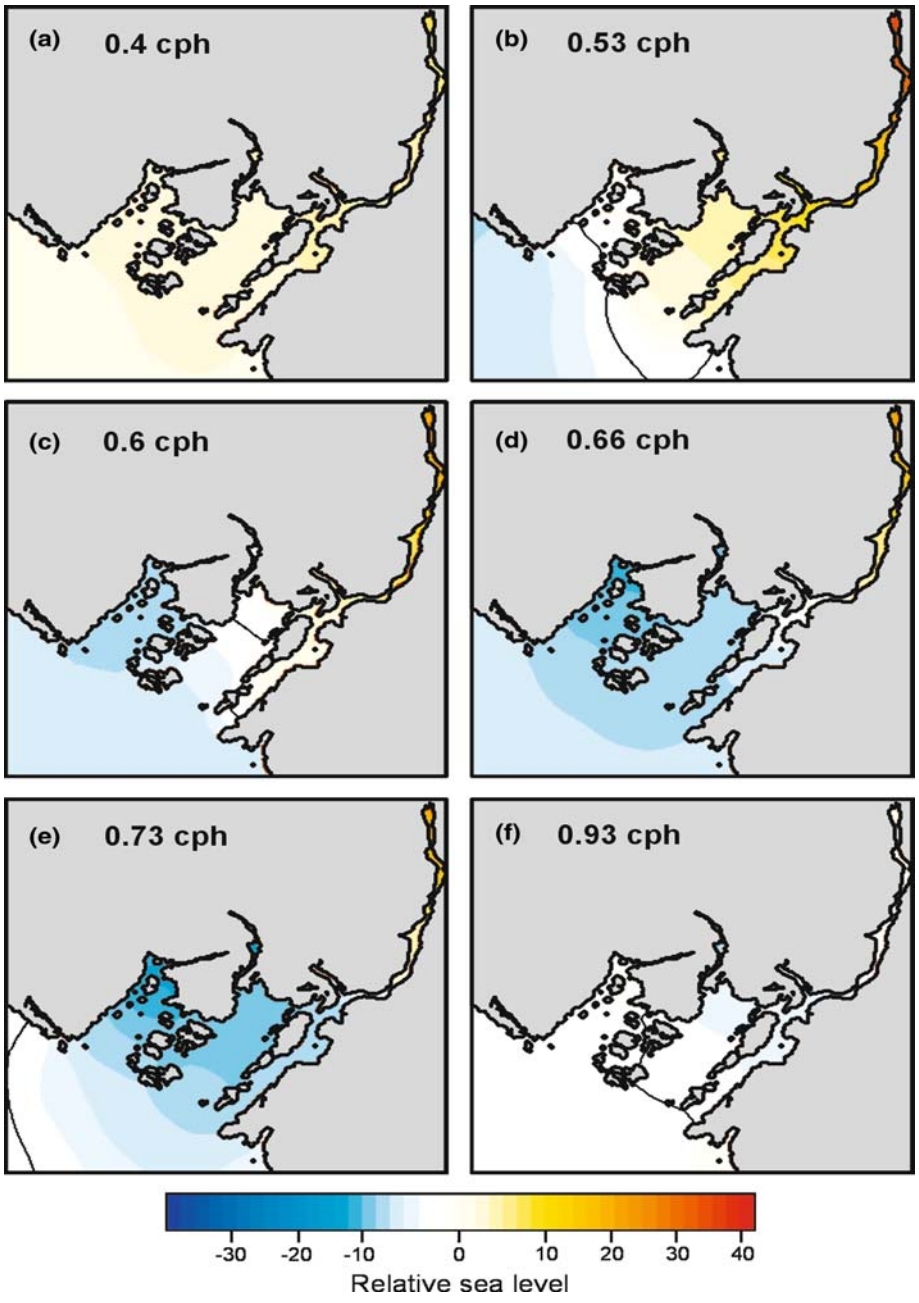

Figure 7
Computed (model A) relative sea-level oscillations in the Barkley Sound and Alberni Inlet system, shown for six select frequencies (marked in each panel).

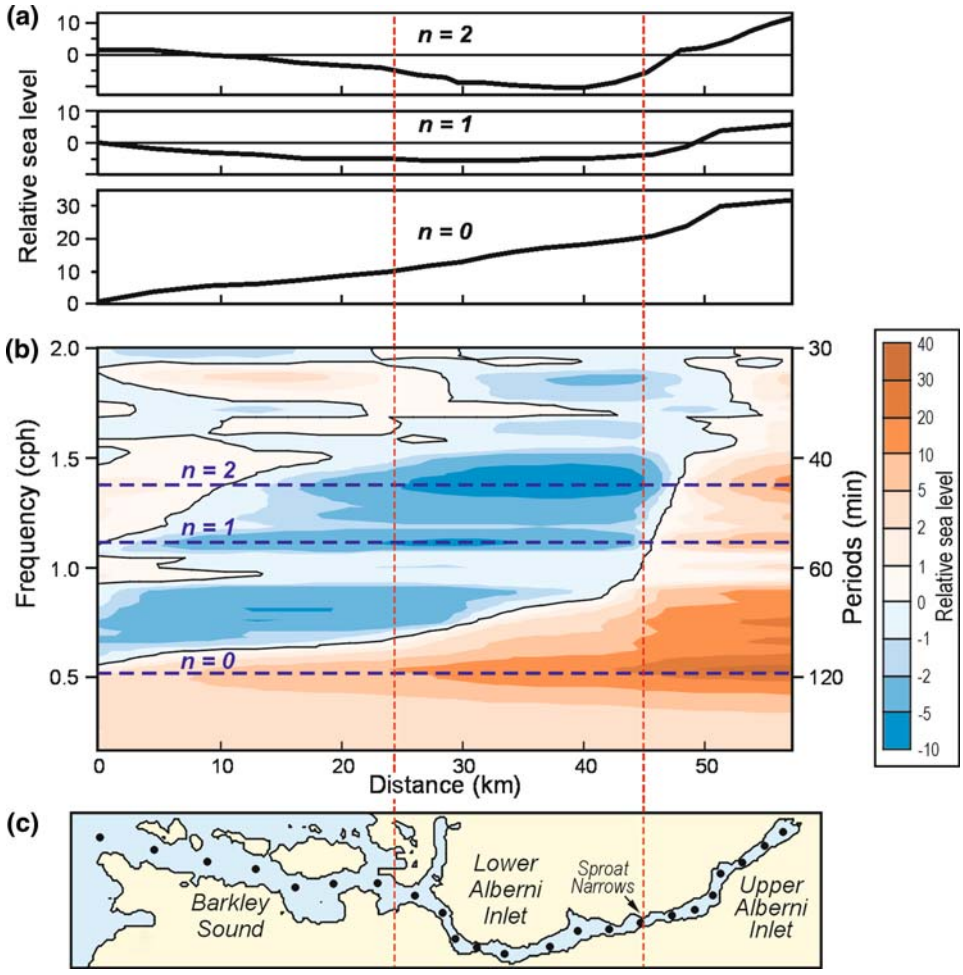

Figure 8

Along-channel computed (model A) structure of sea-level oscillations in Barkley Sound and Alberni Inlet. (a) Computed forms of three first modes (n = 0, 1 and 2). (b) Relative sea-level along-channel heights as a function of frequency with frequencies of the first three modes indicated by horizontal dashed lines. (c) Location of the along-channel transect in Barkley Sound and Alberni Inlet (marked by black solid circles). The red dashed lines separate the three regions: Barkley Sound, lower Alberni Inlet and upper Alberni Inlet.

Sound entrance to Port Alberni (Fig. 8c). This area can be divided into 3 parts: Barkley Sound, the lower Alberni Inlet (up to the Sproat Narrows) and the upper Alberni Inlet.

For low frequencies, up to the 0.9 cph, all three parts show the fundamental mode ($n = 0$) maximum at 112 min (Fig. 8b). As the frequency increases from about 0.55 to 0.8 cph there is still high amplification in much of the area, despite the fact that the nodal line moves inside Barkley Sound. When this line moves past the middle of the lower

Alberni Inlet and the frequency increases beyond 0.9 cph, the oscillations in all three parts decrease in amplitude.

A weak amplification maximum occurs at about 54 min, when another nodal line is located near the entrance of Barkley Sound. However, more significant amplification occurs at 43 min. It is confined mainly to Alberni Inlet, behaving as a classical first-mode asymmetrical pendulum and oscillating between the upper and lower Alberni Inlet, with its nodal line located in the "bottleneck" of Sproat Narrows (Fig. 8c). From the point of view of the complete system, this oscillation can be described as the $n = 2$ mode.

For frequencies beyond 1.5 cph (40 min), Alberni Inlet and Barkley Sound oscillations become decoupled, as the upper Alberni Inlet is almost "blocked" by Sproat Narrows. The lower part of the inlet and Barkley Sound show only weak amplification for these higher frequencies.

5. *Numerical Model B: Tsunami Waves in Alberni Inlet from a Remote Subduction Zone Earthquake*

In the previous two sections we discussed amplification of tsunami waves and excitation of characteristic modes in Alberni Inlet using existing observations of background waves and of tsunami waves from remote earthquakes, as well as from a numerical model (A) forced by stationary auto-regressive spectra. To complete the analysis, we present here results from another model, which uses a scenario of a partial rupture of the Cascadia Subduction Zone (CSZ), the so-called *short-south* scenario of SATAKE *et al*. (2003; see also WANG *et al*., 2003).

The main purpose of the present study is to examine the resonant characteristics of the Alberni Inlet–Barkley Sound system rather than attempt to reproduce exactly the 1964 tsunami waves observed in this system. That is why, and also because we would like to continue the previous study (CHERNIAWSKY *et al*., 2007; thereafter C07), we used in our computations one of the Cascadia Subduction Zone (CSZ) scenarios instead of the 1964 Alaska scenario.

C07 used three CSZ scenarios to simulate tsunami waves and currents in harbors of Ucluelet, Victoria and Esquimalt, located on the southern Vancouver Island Coast (Fig. 1): (1) *long-narrow* (which represents a full rupture of CSZ); (2) *short-north*; and (3) *short-south*. The last two are also plausible scenarios because some megathrust earthquakes involve the rupture of limited segments of a subduction zone. We chose the *short-south* scenario because it also represents a realistic case of a relatively strong earthquake that is likely to generate a well-defined response in Alberni Inlet. At the same time, it is a remote earthquake, allowing us to study relative amplification of distantly-arriving waves in this inlet system.

The *short-south* scenario source region extends about 440 km north to south along the California coast (Fig. 9a). Earthquake magnitude (M_w), equivalent uniform rupture width

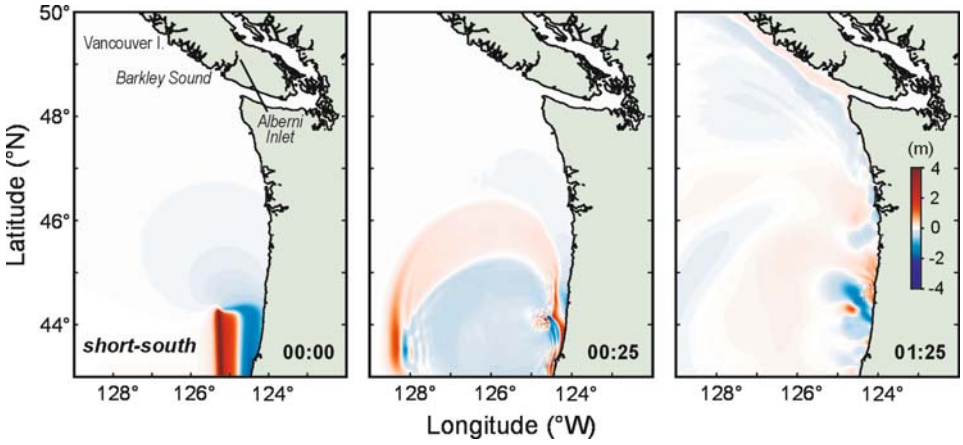

Figure 9

Propagation of the model B simulated tsunami waves from a remote tsunami source off California, generated by the so-called *short-south* CSZ earthquake scenario ($M_w = 8.8$) (SATAKE *et al.*, 2003). The three panels show the wave heights (a) at initial time, (b) at 25 min and (c) at 85 min after the earthquake.

and full-slip zone width for this scenario are 8.8, 56 km, and 37 km, respectively (SATAKE *et al.*, 2003). The resulting tsunami wave energy flux is mostly in a zonal direction, perpendicular to the coast. These waves are expected to produce significant damage in California, Oregon and possibly in Hawaii, but not at coastal locations that are much farther north, such as British Columbia (C07).

The MOST numerical model (TITOV and SYNOLAKIS, 1997), used here and also described in more detail in C07, has three nested grids. The model coarse grid (its grid size $\Delta x \times \Delta y = 1500 \times 1100$ m) extends from 43°N to 50°N, covering the coastlines of Northern California, Oregon, Washington and the southern Vancouver Island (Fig. 9). The coarse and medium (245×185 m) grids are the same as in C07, while the fine grid (outlined with a dashed frame in Fig. 1b) has a horizontal grid size of about 50 m (compared to about 10 m used in C07) and includes Alberni Inlet and a large part of Barkley Sound. This model was integrated for 26 hours using a 0.3-sec time step in its fine grid.

Figure 9 shows initial sea-surface deformation and two snapshots of sea level, after 25 and 85 minutes. The first tsunami waves arrive on southern Vancouver Island coast about 1.5 hours after the earthquake (Fig. 9c). The resulting sea-level maxima at a deep ocean station B1 (at $\sim$1000 m depth; Fig. 1a) and at a station B3 on the shelf off Barkley Sound ($\sim$85 m depth; Fig. 1a) are about 0.15 m and 0.3 m, respectively. As the waves pass through Barkley Sound and into Alberni Inlet, they are amplified. Figure 10 shows nine snapshots on the model fine grid at 10-minute intervals, from 01:40 until 03:00, covering an almost complete wave period after the arrival of the first tsunami wave in Barkley Sound. The minimum and maximum simulated sea-level values during this 80-min period are about $\pm$1.1 m.

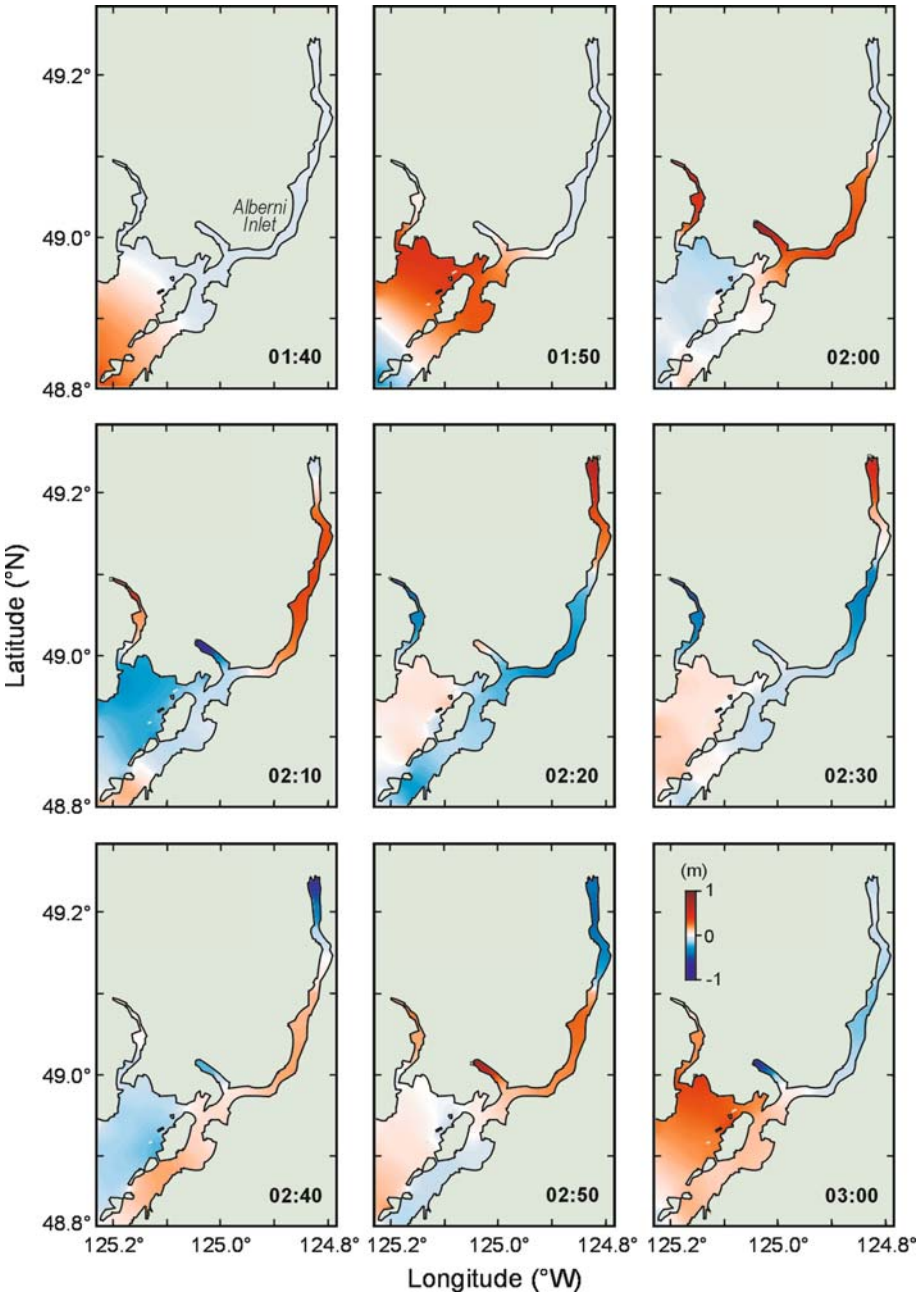

Figure 10

Propagation of tsunami waves inside the model B innermost fine-resolution (50 m) grid in Barkley Sound and Alberni Inlet, shown at 10-minute intervals after the arrival of the first tsunami wave. Time in hours and minutes after the earthquake is marked in each panel (ordered left to right, top to bottom).

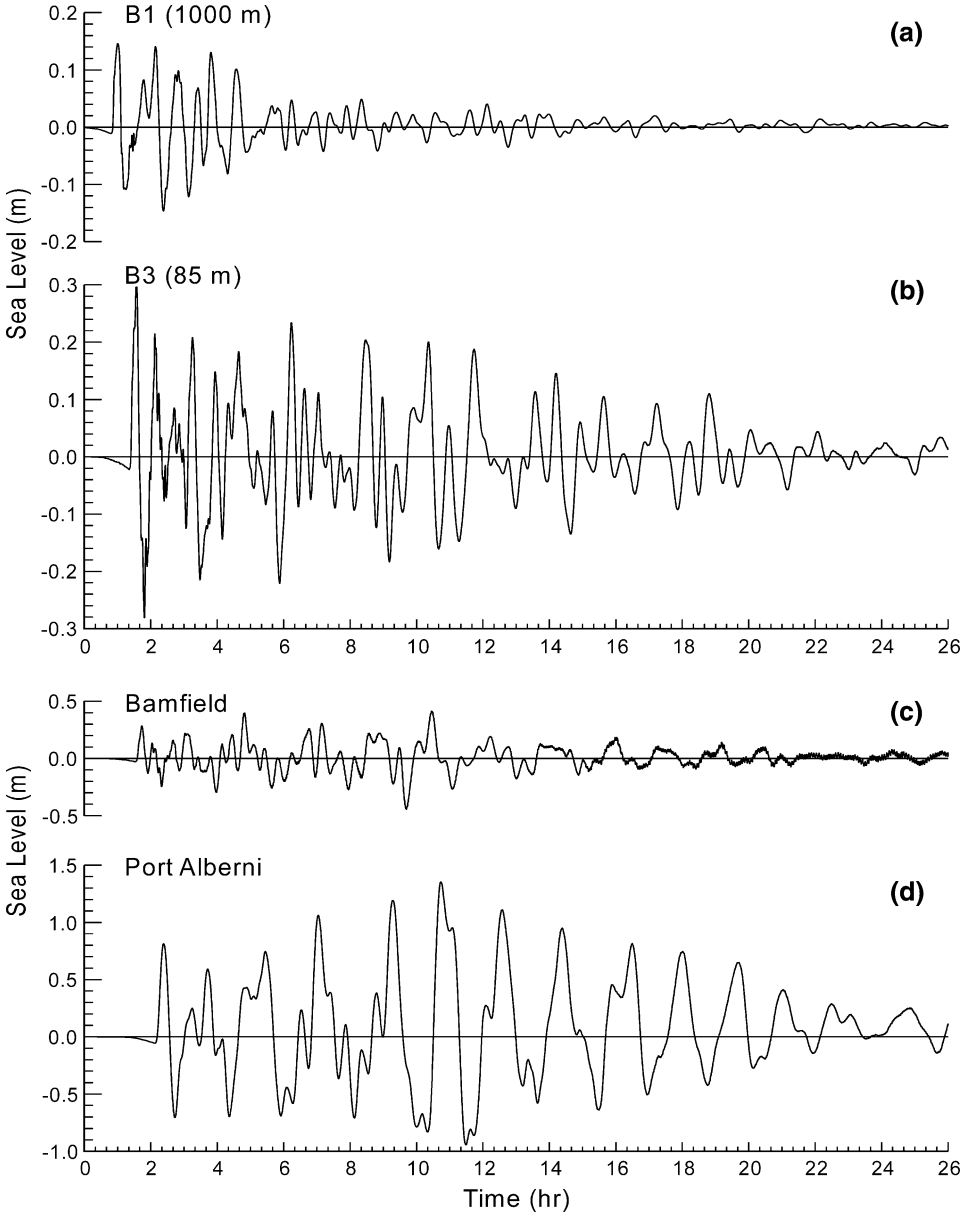

Figure 11
Model B simulated tsunami wave records at four locations: (a) at deep (1000 m) B1 site off Barkley Sound, (b) at B3 site on the continental shelf (85 m) near the entrance to Barkley Sound, (c) near Bamfield and (d) at Port Alberni. Locations of these sites are shown in Figure 1.

Figures 11a-d show time history of sea levels at four select locations: at a deep ocean (1000 m) station off Barkley Sound (B1 in Fig. 1a), at 85-m depth on the continental shelf off Barkley Sound (B3 in Fig. 1a), and at coastal locations near Bamfield and at Port Alberni. The offshore waves (Fig. 11a) decay rather quickly, after about 6 hours, while the waves on the shelf (Fig. 11b), near Bamfield (Fig. 11c) and in Alberni Inlet (Fig. 11d) have considerably longer decay periods. It is notable that the maximum sea level near Port Alberni is about 1.5 m and occurs in this model not during the 1st or the 2nd wave, but during the 6th wave (Fig. 11d), more than 10 hours after the earthquake! If we compare the maximum in Port Alberni to that in deep (1000 m) water, we obtain a maximum amplification factor for this model of about 10. However, by the time (at 10:40) the maximum sea level is reached in Port Alberni (Fig. 11d), amplitude of the waves offshore decays to less than 0.04 m (Fig. 11a).

Maps of the maximum sea level and of the maximum water speed in Barkley Sound and Alberni Inlet during the 26-hr model integration are presented in Fig. 12. The maximum simulated water level of 1.62 m is near Port Alberni (Fig. 12a), though not exactly where the time series shown in Figure 11d was recorded (which explains the

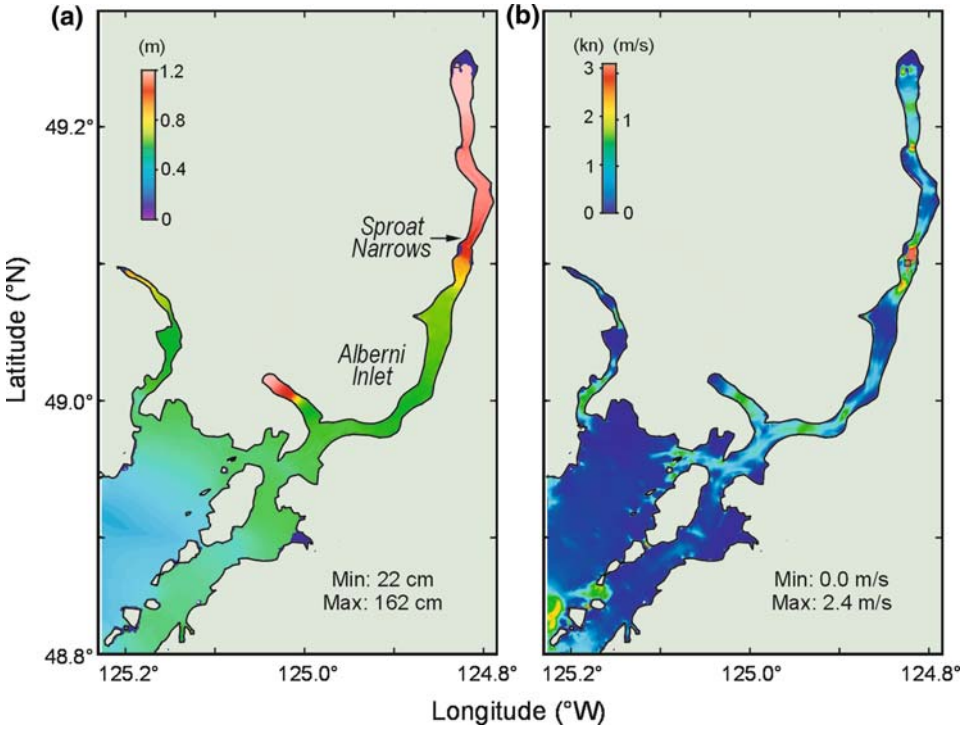

Figure 12
Maps of the model B computed maxima of (a) sea level and (b) water speed in Barkley Sound and Alberni Inlet. The maximum sea level of 1.62 m was near Port Alberni, while the maximum speed of 2.4 m s^{-1} occured in Sproat Narrows.

different maxima in the two figures). The maximum water speed of 2.4 m s^{-1} (5 knots) occurs in the relatively shallow (20–30 m) Sproat Narrows at 49.1°N (Fig. 12b). As was explained in the previous two sections, this channel splits Alberni Inlet into two parts, thus affecting the characteristic modes of the system, which are also apparent in the plot of maximum sea level (Fig. 12a).

The time series of the model B output (Fig. 11) are only 26-hr long and the tsunami wave signals are far from stationary. It is therefore not as straightforward to interpret this model spectrum (Fig. 13), as compared to the higher-quality spectra obtained from long-term observations, or from the much longer integration of the model A, discussed in the previous sections. Nevertheless, the model B spectral peaks compare well to the observed, both for Bamfield (Fig. 13a) and for Port Alberni (Fig. 13b). As was the case for the model A, the main 110-min peak in the model B Port Alberni spectrum is higher than the observed peak, with other peaks appearing as well (67 and 27-min peaks for Bamfield and 47 and 27-min peaks for Port Alberni). The somewhat different peak frequencies can at least in part be attributed to smaller signal to noise ratios and less spectral resolution in the shorter and nonstationary time series from the model B.

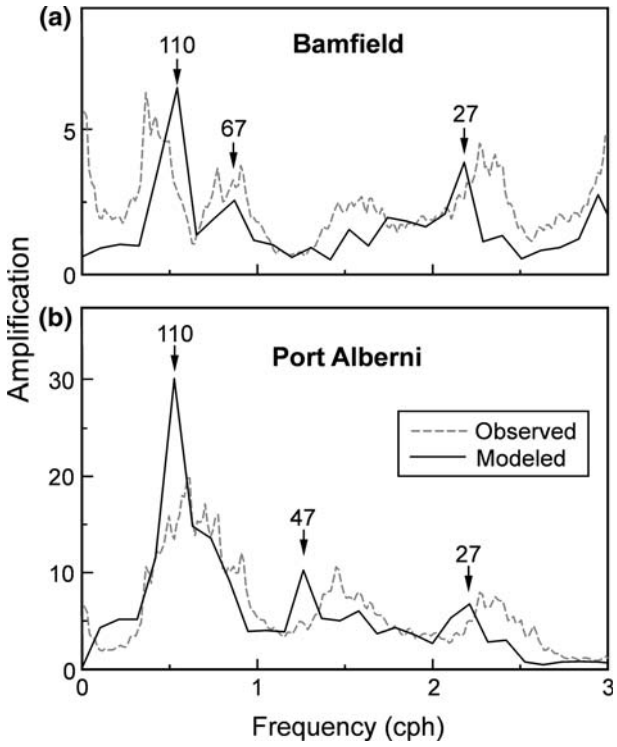

Figure 13
Observed and the model B simulated amplification factor as a function of frequency: (a) at Bamfield and (b) at Port Alberni.

6. Summary and Conclusions

In this work, we have investigated the resonant characteristics and amplification of gravity waves for the tsunami frequency band in Barkley Sound and Alberni Inlet, located on the west coast of Vancouver Island. We analyzed available sea-level observations of two remote tsunamis and of background wave noise, as well as the output from two numerical models for this system. The first model (A) was forced at its open boundary with a stationary autoregressive signal that is similar to the observed background noise. The second model (B) used an initial condition of sea-level deformation from a plausible *short-south* scenario of a Cascadia Subduction Zone earthquake off northern California, producing transient tsunami waves which decay with time.

Analyses of the observations, especially the analyses of background signals from digital tide gauges in Bamfield and Port Alberni, as well as the analysis of spectra from the AR-forced model reveal characteristic features of the frequency response of the system and help to verify the numerical models. For frequencies less than ~ 0.3 cph, spectra from these two tide gauges look almost similar. However, for frequencies higher than ~ 0.3 cph (which include the tsunami frequency band), the two spectra differ significantly, showing wave transformation, modal resonance and amplification in this basin.

Comparison between the observed Port Alberni and Bamfield spectra and their cross-spectra produced very useful results regarding amplification and characteristic modes of the system. We were able to calculate an observed amplification function relative to incoming open-ocean waves, while using an assumption of universal spectra in the ocean. However, data analysis provides results only for specific tide gauge locations (at Port Alberni and Bamfield). It was therefore very informative to use the AR-forced numerical model A, allowing us to study the characteristic modes of the coupled Alberni Inlet–Barkley Sound system and migration of the nodal lines of these modes spanning a wide frequency range over the complete area.

Both the observations and the model A results show that the main features of the frequency response of this area are related to the coupled oscillations in the Barkley Sound-Alberni Inlet system. Because this system has a large length to width ratio, it has a marked quarter-wave resonance, with its fundamental mode ($n = 0$) nodal line located near the open ocean boundary (the entrance to Barkley Sound) at a frequency of about 0.53 cph. The Q-factor of such resonance is related to this ratio. At these frequencies, the system is transparent, i.e., the waves pass freely through its major channels. This also leads to amplification due to the narrowing of the wave path from about 25 km in Barkley Sound entrance to 1–2 km in Alberni Inlet. These two mechanisms combine together to yield a high amplification coefficient over the wide frequency range of 0.4–0.9 cph.

The model A results also show that at the fundamental mode ($n = 0$) frequency of ~ 0.53 cph (period of 112 min), the nodal line of the system is located on the continental shelf near the entrance to Barkley Sound, which is relatively distant from the Alberni Inlet itself (Fig. 1). This is a strong resonant mode, with its amplification factor reaching $A = 12$ at this frequency.

The second prominent amplification peak at 1.4 cph (43 min) is associated with the $n = 2$ mode, while the $n = 1$ mode at about 1.1 cph (54 min) shows only weak amplification. The 43-min mode is directly related to its node being located near Sproat Narrows. The higher frequency modes are not as strong. They are connected with specific smaller-scale features of the inlet system (like Sproat Narrows) and cannot be classified from the point of view of the complete system. Their role in wave transformation is less important, as local amplification at these high frequencies is generally small.

The results from the second model (B) of tsunami waves due to a *short-south* scenario of the Cascadia Subduction Zone earthquake off northern California show spectral characteristics and amplification that are similar to those from model A, or from observed background sea-level data. The nonstationary nature of the model B waves, due to its transient forcing, make direct comparison with the observations or with the model A somewhat inconclusive. However, the model B spectral peaks are at about the same frequencies as in the observed spectra, while its amplification ratios are comparable with those of the model A and the observations. The model B results also show that the maximum tsunami current speeds are in Sproat Narrows, which divides the inlet into two parts, with the largest tsunami waves occurring in the upper Alberni Inlet, especially in the area of Port Alberni.

Acknowledgements

We are grateful to Vasily Titov (PMEL/NOAA) for providing his tsunami model code and to Kelin Wang of the Pacific Geosciences Centre, Natural Resources Canada, for the initial deformation scenario, which was used in the model B. We also thank the Canadian Hydrographic Service for providing the digital bathymetry, Aaron Barlow and Martin Fyfe for their assistance in preparing the gridded data sets for the two models, Richard Thomson for his valuable comments on the first version of the manuscript and Patricia Kimber for preparing the figures for publication. We also extend appreciation to Prof. Kenji Satake, Dr. Lori Dengler and one anonymous reviewer for their helpful comments and suggestions. Fisheries and Oceans Canada have provided the financial support for this investigation. Additional support for Alexander Rabinovich was provided by the Russian Foundation on Basic Research (RFBR), Project 08-05-13582-ofi-c.

References

Anderson, P. S. and Gow, G. A. (2004), *Tsunamis and Coastal Communities in British Columbia: An Assessment of the B.C. Tsunami Warning System and Related Risk Reduction Practices*. 75+xii pp. (Public Safety and Emergency Preparedness Canada, Ottawa, 2004).

Cherniawsky, J. Y., Titov, V. V., Wang, K., and Li, J. -Y (2007), *Numerical simulations of tsunami waves and currents for southern Vancouver Island from a Cascadia megathrust earthquake*. Pure Appl. Geophys. *164*, 465–492.

CLAGUE, J.J. (2001), *Tsunamis*. In *A Synthesis of Geological Hazards in Canada* (ed. G.R. Brooks) Geol. Surv. Canada, Bull. *548*, 27–42.

CLAGUE, J.J., MUNRO, A., and MURTY, T.S. (2003), *Tsunami hazard and risk in Canada*, Natural Hazards *28* (2–3), 407–434.

DJUMAGALIEV, V.A., RABINOVICH, A.B., and FINE, I.V. (1994), *Theoretical and experimental estimation of transfer peculiarities of the Malokurilsk Bay coast, the Island of Shikotan*, Atmos. Oceanic Phys. *30*(5), 680–686.

DUNBAR, D., LEBLOND, P., and MURTY T.S. (1991), *Evaluation of tsunami amplitudes for the Pacific coast of Canada*. Prog. Oceanogr. *26*, 115–177.

EMERY, W.J. and THOMSON, R.E., *Data Analysis Methods in Physical Oceanography*, 2nd and Revised Edition, (Elsevier, Amsterdam) 2001 638 pp.

FILLOUX, J.H., LUTHER, D.S., and CHAVE, A.D., *Update on seafloor pressure and electric field observations from the north-central and northeastern Pacific*. In *Tidal Hydrodynamics*, (ed. B.B. Parker) pp. 617–639, (J. Wiley, New York 1991).

HEBENSTREIT, G.T. and MURTY, T.S. (1989), *Tsunami amplitudes from local earthquakes in the Pacific Northwest Region of North America. Part 1: The outer coast*, Marine Geodesy *13*, 101–146.

HENRY, R.F. and MURTY, T.S. (1972), *Resonance periods of multi-branched inlets with tsunami amplification*, Dep. Environ. Mar. Sci. Div., MS Rep. 28, 47–79.

HENRY, R.F. and MURTY, T.S. (1995), *Tsunami amplification due to resonance in Alberni Inlet: Normal modes*. In *Tsunami: Progress in Prediction, Disaster Prevention and Warning* (eds. Y. Tsushiya and N. Shuto), pp. 117–128, (Kluwer, Dordrecht, 1995).

IMAMURA, F. (1996), *Review of tsunami simulation with a finite difference method*. In *Long Wave Runup Models* (eds. H. Yeh, P. Liu, and C. Synolakis), pp. 25–42 (World Scientific Publishing, Hackensack, N.J, 1996).

KOWALIK, Z. and MURTY, T.S. (1993*), Numerical simulation of two-dimensional tsunami runup*, Marine Geodesy *16*, 87–100.

KULIKOV, E.A., RABINOVICH, A.B., SPIRIN, A.I., POOLE, S.L., and SOLOVIEV, S.L. (1983), *Measurement of tsunamis in the open ocean*, Marine Geodesy *6*(3–4), 311–329.

LANDER, J.F. (1996), Tsunamis affecting Alaska, 1737–1996. USDC/NOAA, Boulder, CO, USA, 195 pp.

MILLER, G.R. (1972), *Relative spectra of tsunamis*, Hawaii Inst. Geophys, HIG-72-8*,* 7 pp.

MURTY, T. S. and BOILARD, L. (1970), *The tsunami in Alberni Inlet caused by the Alaska earthquake of March, 1964*. In *Tsunami in the Pacific Ocean* (ed. W.M. Adams) pp. 165–187 (East West Center Press, Honolulu, HI, 1970).

MURTY, T. S. (1992), *Tsunami threat to the British Columbia coast*. In *Geotechnique and Natural Hazards*, pp. 81–89 (BiTech. Publ., Vancouver, 1992).

MYERS, E.P. and BAPTISTA, A.M. (2001), *Analysis of factors influencing simulations of the 1993 Hokkaido Nansei-Oki and 1964 Alaska tsunamis,* Natural Hazards *23*(1), 1–28.

RABINOVICH, A.B. (1997), *Spectral analysis of tsunami waves: Separation of source and topography effects*, J. Geophys. Res. *102 (C6)*, 12,663–12,676.

RABINOVICH, A.B., MONSERRAT, S., and FINE, I.V. (1999), *Numerical modeling of extreme seiche oscillations in the region of the Balearic Islands*, Oceanology *39*(1), 16–24.

RABINOVICH, A.B**.** and STEPHENSON, F.E. (2004), *Longwave measurements for the coast of British Columbia and improvements to the tsunami warning capability*, Natural Hazards *32*(3), 313–343.

RABINOVICH, A.B., THOMSON, R.E., and STEPHENSON, F.E. (2006), *The Sumatra Tsunami of 26 December 2004 as observed in the North Pacific and North Atlantic Oceans*, Surveys in Geophysics *27*, 647–677.

RABINOVICH, A.B. (2008), *Seiches and harbour oscillations.* In *Handbook of Coastal and Ocean Engineering* (ed. Y.C. Kim) (World Scientific, Singapore) (in press).

SATAKE, K. (1995), *Linear and nonlinear computations of the 1992 Nicaragua earthquake tsunami*, Pure Appl. Geophys. 144, 455–470.

SATAKE, K., Wang, K., and Atwater, B.F. (2003), *Fault slip and seismic moment of the 1700 Cascadia earthquake inferred from Japanese tsunami descriptions*, J. Geophys. Res. 108(B11), doi:10.1029/2003JB002521.

SPAETH, M.G. and BERKMAN, S.C. (1967), *The tsunami of March 28, 1964, as recorded at tide stations*, ESSA Technical report C&GS *33*. 86 pp.

Stephenson, F., Rabinovich, A.B., Solovieva, O.N., Kulikov, E.A., and Yakovenko, O.I. (2007), *Catalogue of Tsunamis, British Columbia, Canada: 1700–2007*, Preprint, P.P. Shirshov Institute of Oceanology, Moscow, Russia, 133 pp.

Stephenson, F. and Rabinovich, A.B. (2009), *Tsunamis on the Pacific Coast of Canada recorded during 1994–2007*, Pure Appl. Geophys. submitted.

Titov, V. V. and Synolakis, C. E. (1993), *A numerical study of wave runup of the September 2, 1992 Nicaraguan tsunami,* Proc. IUGG/IOC Inter. Tsunami Symposium (Wakayama, Japan, 1993) pp. 627–635.

Titov, V.V. and Synolakis, C.E. (1997), *Extreme inundation flows during the Hokkaido–Nansei–Oki tsunami*, Geophys. Res. Lett. *24*(11), 1315–1318.

Vilibić, I., Monserrat, S., Rabinovich, A.B., and Mihanović, H. (2008), *Numerical modelling of the destructive meteotsunami of 15 June 2006 on the coast of the Balearic Islands*, Pure Appl. Geophys. doi 10.1007/s00024-008-0426-5.

Wang, K., Wells, R., Mazzotti, S., Hyndman, R.D., and Sagiya, T. (2003), *A revised dislocation model of interseismic deformation of the Cascadia subduction zone*, J. Geophys. Res. *108*(B1), doi:10.1029/2001JB001227.

White, W.R.H. (1966), *The Alaska Earthquake – Its effect in Canada*, Can. Geogr. J., 210–219.

Whitmore, P.M. (1993), *Expected tsunami amplitudes and currents along the North American coast for Cascadia Subduction Zone earthquakes*, Natural Hazards *8*(1), 59–73.

Wigen, S.O., *Historical studies of tsunamis at Tofino*, Canada. in *Tsunamis – Their Science and Engineering* (ed. K. Iida and T. Kawasaki,) (Terra Sci. Publ. Comp., Tokyo, Japan (1983)). pp. 105–119.

Wigen, S. O. and White, W. R. H. (1964), *Tsunami of March 27–29, 1964, west coast of Canada*, Unpublished manuscript, 6 pp. (Department of Mines and Technical Surveys, Ottawa, 1964).

(Received April 9, 2008, revised July 9, 2008)
Published Online First: December 19, 2008